CHARACTERIZATION OF PORE TO PORE DIFFUSIVE EXCHANGE USING NMR T_2-STORE-T_2 2D EXPERIMENTS

M. FLEURY

Institut Français du Pétrole

This paper was prepared for presentation at the International Symposium of the Society of Core Analysts held in Noordwijk, The Netherlands 27-30 September, 2009

ABSTRACT

Low field NMR T_2 distribution is an efficient tool for characterizing pore size distribution in porous media. For multimodal systems, a new technique called T_2-store-T_2 allows the analysis of diffusional pore to pore exchange that is extremely useful for the characterization of connectivity. This technique uses 2D inverse Laplace techniques and produces T_2-T_2 maps. Qualitatively, a system is coupled when off-diagonal peaks are observed. Based on an analytical solution describing diffusional coupling between two pore sizes, we propose defining a coupling factor that quantify the degree of coupling between two pore populations, and allows an easy understanding of the complex analytical solution. This analysis allows understanding 1D T_2 experiments as well, and provides some limitations of the T_2 characterization when interpreted as a pore size distribution. We provide examples of bimodal pore structures in which we applied our methodology: a clay gel system, a shaly sandstone and a double porosity carbonate. These systems are also described by conventional techniques (mercury injection, SEM visualization) and illustrate weak, intermediate and strong coupling. Despite the presence of distribution of pore sizes, the two pore system exchange model gives satisfactory results for the quantitative analysis of the coupling and T_2-store-T_2 experiments. However, in carbonates, more complex exchanges can occur between micro, meso and macro pores.

INTRODUCTION

Diffusional pore coupling is an issue of practical importance for the correct interpretation of NMR pore size distribution performed in the laboratory and in situ. At the extreme situation, a multimodal pore system may appear as unimodal due to pore to pore diffusional exchange and this has important interpretation consequences. This phenomenon has been studied initially to explain the temperature dependence of NMR relaxation data. Indeed, relaxation in porous media should not depend on temperature and this fact was put forward to justify the surface dominated regime [1]. However, in carbonates, a significant temperature dependence can occur, typically when comparing laboratory and log data performed respectively at 20 and 100°C. This is a direct effect of pore coupling and a solution to predict the shift of the T_2 distributions was proposed [2]. Later, Anand et al. [3,4] proposed a 1D geometric model and a coupling parameter to describe the pore to pore coupling phenomenon and applied it to various situations. For bimodal pore systems, the shift of macro and micro pore NMR peaks can be predicted as a function of the coupling parameter comparing the characteristic relaxation rate to the diffusion rate.

From the NMR point of view, the methods for observing the modification of the environment of spin carrying molecules has been evidenced very early in the

development of NMR [5]. At high field, the analysis of the chemical exchange is now a common practice, for example in the exchange spectroscopy technique EXSY [6] that uses very similar principle as described here. The results of these experiments is a 2D map of chemical shift in which off-diagonal peaks signify a change of chemical environment after a chosen exchange time. At low field, the observation of the modification of the spin carrying molecules in terms of relaxation is recent. Simultaneously, two groups [7, 8] proposed new NMR sequences to detect the relaxation exchange of molecules in the case of a cement paste and a sandstone. The experiment consists of two T_2 relaxation periods with a variable exchange time sandwiched between them. When analyzing the resulting 2D T_2-T_2 maps, the pore coupling is evidenced by off-diagonal peaks. The motions of molecules can be observed only if a surface relaxivity contrast exists between T_1 and T_2 [7, 9] which is usually the case in porous media. More generally, the existence of off-diagonal peaks can also be analyzed from the resolution of eigenvalues of the underlying Bloch-Torrey diffusion equations and some general behavior can be deduced [9].

In this work, we first analyse the analytical solution proposed by Montheillet et al. [7] and propose a coupling parameter based uniquely on NMR measurable factors to quantify the degree of coupling between two pore sizes. Then, the method is applied to different systems with a large range of sizes, from nanometers to tens of microns. We study the pore to pore exchange in a natural bimodal model system composed of flocculated clay particles, and samples typical of oil bearing rocks: a high permeability sandstone containing clays and two complex carbonates.

BACKGROUND

We first consider the case of complete coupling using a simple fast exchange model. Consider two porous zones in a porous media (Fig. 1), typically representative of micro (subscript a) and macropores (subscript b). For simplicity, we will assume a unique pore size in each zone. In these conditions, the NMR relaxation time in the surface dominated regime in the absence of coupling will be proportional to the volume to surface ratio of the macro pores $T_{2b} \propto V_b/S_b$ and micro pores $T_{2a} \propto V_a/S_a$. The measured distribution will be bimodal. In this case, diffusive molecular motions are such that the magnetization has decreased to zero before the molecules can travel to a different porosity zone.

In the case of complete coupling, molecules explore both environments during the typical life time of the magnetization. Assuming that relaxation is still in the fast diffusion regime, the observed relaxation time T_2^+ (the notation is linked to the theory described later) is then proportional to the total volume to surface ratio according to:

$$T_2^+ \propto \frac{V_T}{S_T} = \frac{V_a + V_b}{S_a + S_b} \tag{1}$$

Each volume V_a and V_b corresponds to a magnetization M_a^0 and M_b^0. Assuming a unique surface relaxivity for both a and b zones, the observed relaxation time T_2^+ is unique and smaller than the macro pore peak T_{2b} according to:

$$\frac{T_2^+}{T_{2b}} = \frac{M_a^0 + M_b^0}{\frac{T_{2b}}{T_{2a}} M_a^0 + M_b^0} \tag{2}$$

For example, when the pore sizes are different by a factor of 10 (T_{2b}/T_{2a}=10), the observed single relaxation time $T_2^+ = 0.2T_{2b}$ when $M_a^0 = M_b^0$. The relaxation time T_2^+ is closer to the micro-pore peak than the macro-pore because there is much more surface in the microporosity.

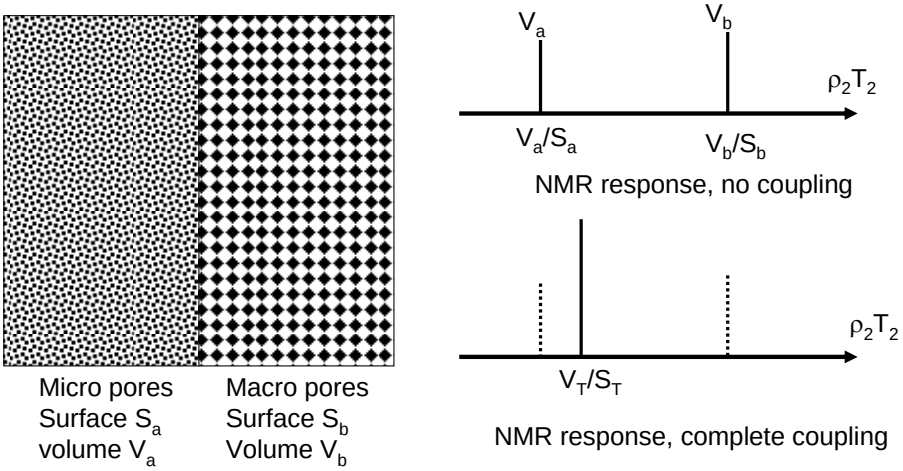

Fig. 1: Illustration of the pore coupling effect on 1D T_2 relaxation time distributions. The pore structure information may be lost; micro and macro pores can no longer be identified in the case of complete coupling.

If the coupling is intermediate, we now use the theory developed by Monteilhet et al. [7] describing the full details of the diffusional coupling between two zones a and b, and we show that a single parameter can be build to characterize the degree of coupling. For spin-spin relaxation, the system of coupled differential equations is given by:

$$\begin{aligned} \frac{dM_a}{dt} &= -k_a M_a + k_b M_b - R_2^a M_a \\ \frac{dM_b}{dt} &= -k_b M_b + k_a M_a - R_2^b M_b \end{aligned} \tag{3}$$

where $k_{a,b}$ is the exchange rate, $R_2^{a,b}$ is the nuclear spin-spin relaxation rate (=$1/T_{2a,b}$) of each zone in the absence of coupling. At t=0, the magnetization in each reservoir is $M_{a,b}^0$; the exchange rates $k_{a,b}$ are linked by the balance equation:

$$k_a M_a^0 = k_b M_b^0 \tag{4}$$

The system of equations (3) was solved analytically [7] in the specific context of the T_2-store-T_2 sequence described later. The observed relaxation rates $s_{1,2}^{+/-}$ ($=1/T_{1,2}^{+/-}$) in the T_2-T_2 map (Fig. 2) are given by :

$$s_{1,2}^{+/-} = -\frac{1}{2}(R_{1,2}^a + k_a + R_{1,2}^b + k_b) \pm \frac{1}{2}\sqrt{(R_{1,2}^a + k_a + R_{1,2}^b + k_b)^2 - 4\left\{(R_{1,2}^a + k_a)(R_{1,2}^b + k_b) - k_a k_b\right\}} \tag{5}$$

The observed amplitudes of the diagonal peaks P^{++} and P^{--}, and off-diagonal peaks P^{+-} and P^{-+}, are function of an exchange time t_e defined later:

$$\begin{aligned} P^{++} &= C_1 \exp(s_1^+ t_e) + C_2 \exp(s_1^- t_e) \\ P^{--} &= C_3 \exp(s_1^+ t_e) + C_4 \exp(s_1^- t_e) \\ P^{+-} &= P^{-+} = C_5 \exp(s_1^+ t_e) + C_6 \exp(s_1^- t_e) \end{aligned} \tag{6}$$

where the coefficients C_1 to C_6 are complicated functions of $s_{1,2}^{+/-}$, $M_{a,b}^{0}$, $R_{1,2}^{a,b}$ and $k_{a,b}$ (see appendix 1). These peaks can be observed experimentally using 2D inverse Laplace techniques. The above model can be used to show the shift of the micro and macro pore peaks in a 1D NMR CPMG relaxation experiment, and to explore the behavior of 2D experiments for different degrees of coupling.

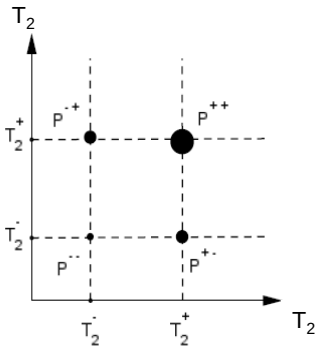

Fig. 2: Illustration of the positions and amplitudes of diagonal and off-diagonal peaks as a result of diffusional coupling between two reservoirs, as measured in a T_2-store-T_2 experiment.

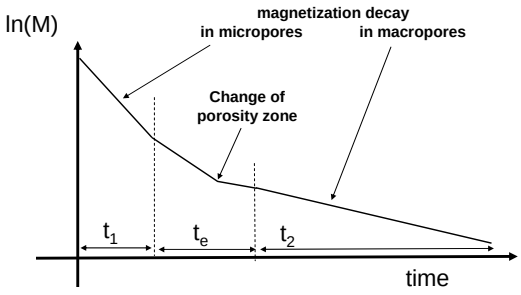

Fig. 3: Principle of the T_2-store-T_2 sequence to observe diffusional coupling (see text).

NMR sequence and 2D inversion

The T_2-store-T_2 sequence used is essentially a succession of two CMPG sequences separated by a storage time te:

$$P_{90} - (\tau - P_{180} - \tau - \text{echo} -)_m - \quad P_{90} - t_e - P_{90} \quad - (\tau - P_{180} - \tau - \text{echo}_{acq} -)_n$$

Essentially, the relaxation is first observed using a CPMG sequence of variable length. Then, the magnetization is stored along the z-axis (T_1 relaxation) to allow spin bearing molecules to move by diffusion in a different environment (a different pore system). Also, because the T_1 surface relaxivity is slightly different, the relaxation decay during the storage or exchange period is different. Finally, the magnetization is returned to the x-y plane and the decay recorded. The result of the experiment is a T_2-T_2 map containing 4 peaks in the case of coupling (Fig. 2). The principle of the experiment can also be illustrated by considering a single spin carrying molecule traveling from a micro-porous to a macro-porous zone. The magnetization decay (Fig. 3) has a different slope at $t=t_1$ due to T_1 relaxation. During the exchange period, there is a change of slope due to relaxation in the macro-porosity. Finally, at the end of the exchange period, there is another change of slope due to T_2 relaxation in the macroporosity. By varying t_1 and the exchange period t_e, one can detect the change of relaxation environment, i.e. the shift from micro to macroporosity. Hence, the decay has two components T_2^+ and T_2^- in 2D T_2-T_2 map.

In practice, only the echo intensities in the second part of the sequence are acquired, yielding a two dimensional data set of size (m,n) such that the recorded magnetization is a two dimensional function of t_1 and t_2:

$$M(t_1,t_2) = A_{xy}\exp(-t_1/T_{2x})\exp(-t_e/T_1)\exp(-t_3/T_{2y}) \ , \ t_1 = 2m\tau \ , \ \ t_3 = 2n\tau \qquad (7)$$

It is usually necessary to have small τ values to properly catch short relaxation times but this would result in a huge number of pulses when large and small relaxation times are present simultaneously such as in our carbonate systems. To limit the total number of pulses to about 10000 (to avoid a potential heating of the sample and unstability of

the power amplifier), the inter pulse time τ is increased gradually from an initial value of 30 μs up to 100 μs (or more depending on the largest relaxation time present in the sample). Then, it stays at a constant value. During the second CPMG sequence, typically 5000 echo maximum are recorded (the value of n is tuned such as to obtain a signal decaying to zero, as usually performed in a single CPMG sequence). Then this signal is compressed by averaging all echo maximum into 40 predefined bins having a constant log spacing in time (with origin the third P_{90}), yielding a compressed time series t_c. For the first CPMG sequence, only the m values corresponding to the 40 values of t_c are used. Hence, the two dimensional data set acquired reduces finally to a 40x40 matrix. The advantage of this protocol is the large increase of signal to noise ratio for intermediate and large relaxation times due to compression.

The solutions described in Eq. (5) and (6) are only valid if a +/-z phase cycling is performed when averaging several signals. If this is not performed, many off-diagonal peaks may be observed, even in a single pore [9]. Adding this phase cycling to the usual CYCLOP phase cycling, a minimum of 8 scans is necessary. The total acquisition time is equivalent to about 40 1D CPMG sequences. Depending on the repeat delay time, the duration of the acquisition varies from 1 to 10h.

We analyzed the relaxation data using our own 2D Laplace inverse Laplace routine written in MATLAB. A 40x40 relaxation time matrix is generally used and the regularization parameter is determined using a method similar to the 1D calculation.

Experiments were performed on a MARAN-ULTRA 23.7 MHz from Oxford Instruments equipped with a 18 mm proton probe. The samples are small cylinders of diameter 15 mm and length 20 mm. For the gels, we used a glass container of similar size.

Coupling parameter

Due to the complicated solution of equation (3), it is rather difficult to analyze the effect of the numerous parameters included in the system. For this purpose, we suggest to use the following coupling parameter:

$$\alpha = \frac{(average\ exchange\ rate)}{(micropore\ relaxation\ rate)} = 2(k_a + k_b)T_{2a} \tag{8}$$

There are other possibilities for defining a coupling parameter. Here, we base our parameter on the micropore relaxation rate (or the smallest pores) because microporosity is a major source of relaxation due to the much larger amount of surface compared to macroporosity. We will also see that the use of this parameter greatly simplifies the analysis of the system. Using equations (4), (5) and (6), we calculated four quantities of practical interest by varying the exchange rate k_a by several orders of magnitude; random choices of the pore size ratio T_{2b}/T_{2a} and magnetization ratio M_a^0/M_b^0 were selected in the intervals [5, 50] and [0.05, 1] respectively. This means that we consider situations where the micro and macro pores are well separated and micro porosity does not exceeds macro porosity. We used T_1/T_2 = 1.5, a typical value for sandstones and carbonates at a Larmor frequency of 2 MHz.

The 4 quantities of interest are plotted in Fig. 4:

- the ratio P^{--}/M_a^0 calculated at t_e=0 represents the observed microporosity amplitude relative to the true one in a 1D experiment. It mostly follows a S shaped curve that has been found using a very different approach [3]. To go from a weak coupling

(α<0.1) to a strong coupling (α>10), the parameter α must vary by two orders of magnitude,

- the ratio $2P^{+-}/P_{tot}$ calculated at t_e=T_{2b} represents the amplitude of the relative off-diagonal peak intensity in a 2D experiment. With the choice T_1/T_2 = 1.5, it has a maximum at $\alpha \cong 1$; this maximum will occur at smaller α when increasing the ratio T_1/T_2 (at the extreme value of 4, the maximum occurs at 0.6). For strongly coupled systems (α>10), it means that the 2D T_2-store-T_2 experiment is unable to evidence the coupling. One must lower the value of α using a fluid of lower diffusivity,
- concerning relaxation times, the ratio T_2^+/T_{2b} expresses the deviation of the macropore relaxation time relative to its true value without coupling. It depends both on α and the magnetization and relaxation time ratio M_a^0/M_b^0 and T_{2b}/T_{2a} respectively. We also verified that, for large α:

$$\frac{T_2^+(\alpha \to \infty)}{T_{2b}} = \frac{M_a^0 + M_b^0}{\frac{T_{2b}}{T_{2a}} M_a^0 + M_b^0} \tag{9}$$

which corresponds to the value given in Eq. (2) using the simple model explained above,

- finally, the ratio T_2^-/T_{2a} expresses the shift of the micro pore relaxation time relative to its value without coupling. Surprisingly, the micro pore peak is shifted to smaller T_2 values (Fig. 4) as the coupling coefficient increases, whereas one would have intuitively expected a gradual merging of the micro and macro pore peaks. This behavior has been clearly observed experimentally in model systems and predicted [3].

It can be shown that off-diagonal peaks are increasing function of t_e and are maximum at the observed relaxation time T_2^+. Therefore, if no off-diagonal peaks are observed at t_e=T_2^+, the system is uncoupled.

RESULTS

We studied 3 systems showing a bimodal pore structure in which diffusional exchange are suspected to modify the pore structure information inferred from 1D relaxation time distribution.

Smectite gels (model system)

The first system consists of smectite clay particles that have aggregated due to inter particle interactions occurring at high salinity (0.1 mol/L $CaCl_2$) and high clay concentration. A full study of diffusion properties [10] shows an exponential decrease of the effective diffusion coefficient as a function of clay fraction. When flocculated, the T_2 distribution is bimodal; the lowest mode corresponds to the intra-flock spacing (about 1 nm, see figure 8 in ref. 10) and the highest to the inter-flock spacing (about 10 nm), the latter varying with the amount of clay. Given the very small pore sizes in these systems, diffusional coupling may strongly affect the T_2 distribution and result in wrong conclusions about the inter and intra-flocks fraction.

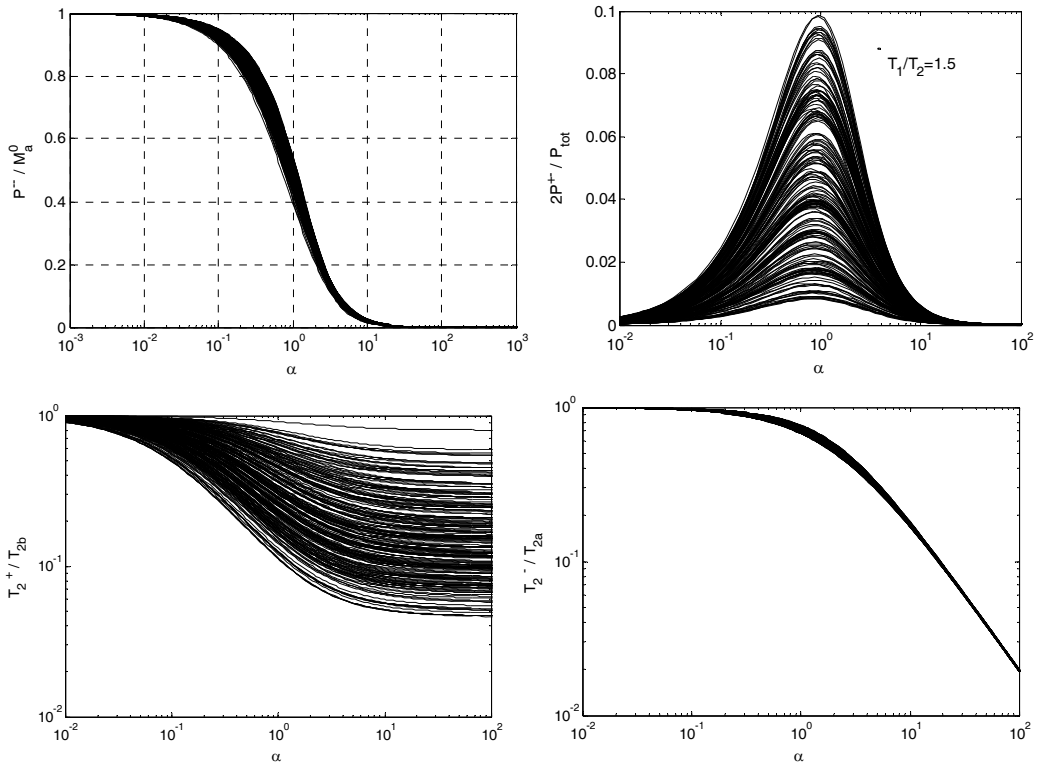

Fig. 4: Study of 4 quantities of interest as a function of the coupling parameter α when the ratio T_{2b}/T_{2a} varies from 5 up to 50, and M_a^0 / M_b^0 from 0.05 up to 1 (T_1/T_2 = 1.5). Random combinations of these two ratios were chosen to calculate the curves. P^{--} / M_a^0: amplitude ratio of the observed microporosity peak to the true amplitude at t_e=0 ; $2P^{-+} / P_{tot}$: amplitude ratio of the off-diagonal peak to the macroporosity peak at t_e=T_{2b}; T_2^+ / T_{2b}: deviation of the macropore relaxation time relative to its true value; T_2^- / T_{2a}: deviation of the micropore relaxation time relative to its true value.

The T_2-store-T_2 experiments were performed on the 30% clay fraction sample for increasing values of the storage time t_e, from 0.5 ms up 10 ms. The 2D maps (Fig. 5) indicate no diagonal peaks at short exchange time (te=0.5 ms) but they gradually appear when increasing the exchange time. The four peaks form a square pattern as expected but the square is not perfect due to uncertainties in the 2D analysis. We also measured T_1 and T_2 distributions and determined that T_1/T_2 = 1.8.

The analysis of the peak intensities as a function of the storage time not detailed here allows the calculation of k_a=0.06, k_b=0.011, $M_a^0/(M_a^0+M_b^0)$=0.155, T_{2b}=11 ms, T_{2a}=2ms. Hence, the degree of coupling is α=0.28. According to Fig. 4, this system is weakly coupled and intraflocks porosity fraction is underestimated by about 10% only.

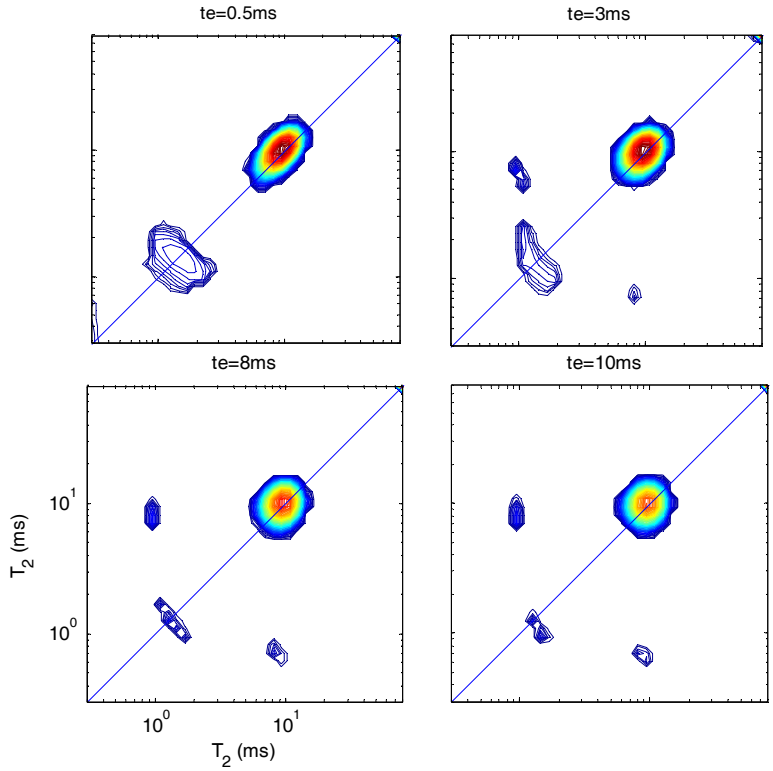

Fig. 5: T_2-store-T_2 relaxation maps for a smectite gel at a clay fraction of 30 %, as a function of the exchange time t_e. The position of the micro and macropore peaks are independent of t_e (T_2^+=9.7 ms, T_2^-=1.4 ms).

Shaly sandstone (Vosges sandstone).

This case is typical of natural sandstones containing a variable amount of clays, either filling the pores or lining at their surface. The estimation of the pore volume fraction occupied by water in clays is of practical industrial importance because it is directly related to the potential of an oil reservoir in terms of hydrocarbon in place. Compared to the previous example, the pore sizes are changed by several orders of magnitude. Typically, clay pore sizes in such natural systems is around 1 μm or less and intergranular spacing is of the order of 10 μm. However, from NMR, the separation between water trapped in clays (clay bound water) and intergranular water is usually not well defined, as shown by the 1D projection of the 2D map at short exchange time in Fig. 6. It is usually considered that a cut-off around 10 ms gives reasonable estimation of clay bound water [11].

The T_2-T_2 maps calculated at a long exchange time (t_e=90 ms, Fig. 6) indicate clearly an exchange between clays and intergranular porosity (i.e. between pores at T_2^-=2 ms and T_2^+=50 ms indicated by the square pattern). In a similar way as for the smectite gel, we analyzed the intensities as a function of the exchange time t_e. In this case, we subdivided the T_2 maps into 4 regions to define off and on-diagonal intensities (Fig. 6).

In this case, the intensities P^{++}, P^{--}, P^{+-} and P^{-+} are the sum of the amplitudes in each sub-region. We found k_a=0.02 ms^{-1}, k_b=0.016 ms^{-1}, $M_a^0/(M_a^0+M_b^0)$=0.45, T_{2b}=200 ms, T_{2a}=10 ms. The T_1/T_2 ratio was set at 1.8. Hence, the degree of coupling

α=0.73 is weak to intermediate. The back calculated values of T_2^- and T_2^+ are respectively 8 and 55 ms, close to the observed values (2 and 50 ms). Hence, the intergranular pore size (or more exactly the V/S ratio) is underestimated by a factor of 4 on the 1D distribution.

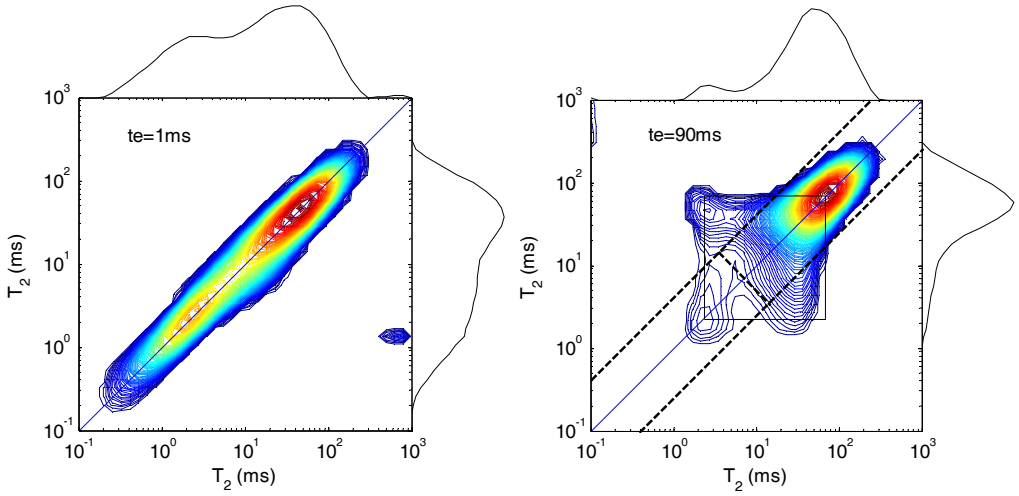

Fig. 6: T_2-store-T_2 relaxation maps for a Vosges sandstone sample for two values of the exchange time t_e. Porosity 22 % and permeability: 210 mD. The clay (micropore) and intergranular (macropore) peaks are centered around T_2^- =2 ms and T_2^+=50 ms respectively. The square pattern indicate the coupling, and the dashed lines the sub-regions for calculating peak intensities.

A double porosity carbonate

The sample used here is part of a larger study comparing NMR T_2 distributions and pore throat size distributions deduced from mercury injection experiments (MICP), with the help of visual examination of the pore structure from thin sections and scanning electron microscopy (SEM) [12]. In this work, it was established that microporosity defined in the petrographical sense, is the volume accessible through throat diameters smaller than 2 μm and correspond to relaxation times smaller than 200 ms in the T_2 distribution.

A careful observation of the porous structure may give good indication of the existence of pore coupling. In the case of the Lavoux limestone (Fig. 7, left), microporosity is located in well identified spherical structures (oolithes) without cementation at their surface. In this case, the bimodal MICP signature (Fig. 7, right) is in contradiction with the 1D NMR when saturated with water (Fig. 8, left). Indeed, the MICP indicates that about 50% of the pore volume is accessible through throat diameters below 2 μm. The NMR distribution indicates a wide distribution with a small peak around 2 ms representing only 10% of the pore volume. The 2D map indicates an exchange between population located at 30 and 2 ms. Clearly, there exist very large pores (of the order of 100 μm) that should have a large relaxation time (1000 ms) similar to the previous case. Therefore, this system is strongly coupled and the pore size information from 1D T_2 distribution is lost. To decrease the degree of coupling, the saturating fluid was replaced by a mixture of water and glycerol to a weight ratio of 36:64. Hence, the diffusivity is reduced by one order of magnitude (from 2.6 10^{-9} m^2/s down to 0.18 10^{-9} m^2/s at 30°C, as measured by PFG-NMR). The liquid bulk relaxation time is also reduced (from 2700

down to 380 ms) but is sufficiently large to allow the observation of large pores. In these conditions, we observed a tri modal 1D distribution more representative of the texture observed by SEM. When performing the exchange experiment using a similar exchange time (30 ms), we see two couples of diagonal peaks indicating an exchange between populations located at 30 and 2 ms, and 300 and 2 ms, but no exchange between populations at 300 and 30 ms. We interpret these observations in terms of the structure revealed by SEM visualization (Fig. 7): oolithes contain microporosity but also intermediate size pores (that could be labeled mesoporosity) in their centers. Hence the exchange between meso and macro pores has a large time constant preventing the observation of off-diagonal peaks. It is also consistent with the observation of two distinct peaks in the MICP distribution: meso porosity is only accessible through micro porosity located around the oolithes.

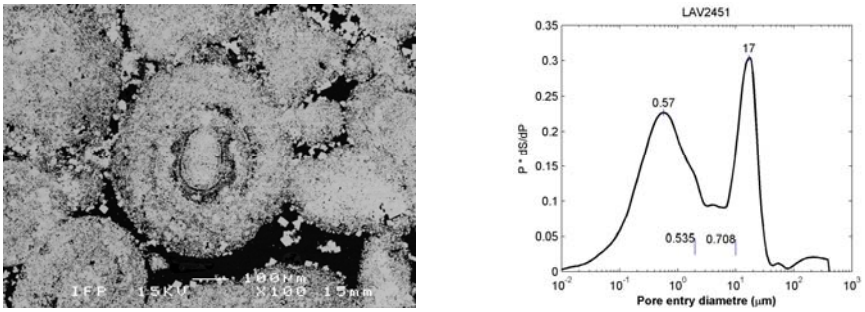

Fig. 7: Characterization of a Lavoux limestone sample. Left: SEM visualization, Right: mercury injection capillary pressure curve (MICP). Porosity: 24 %, permeability: 19 mD. The two pore size structure is evidenced by the bimodal MICP pore entry size distribution.

For both saturating liquids, we calculated the peak intensities in a similar way as for the Vosges sandstone and attempted to calculate the coupling coefficients and exchange rates. These attempts were not successful and yielded inconsistent values of T_2^- and T_2^+ when compared to the observed peak center position. This not surprising because the model only takes into account two pore populations. However, a rough estimation of the coupling coefficient can be made by comparing the experiments with water and water/glycerol: the exchange rate being proportional to diffusivity and decreased by a factor of ten, we have necessarily a coupling coefficient in the range 1 to 10 for water experiment, and 0.1 to 1 for the water/glycerol mixture experiment.

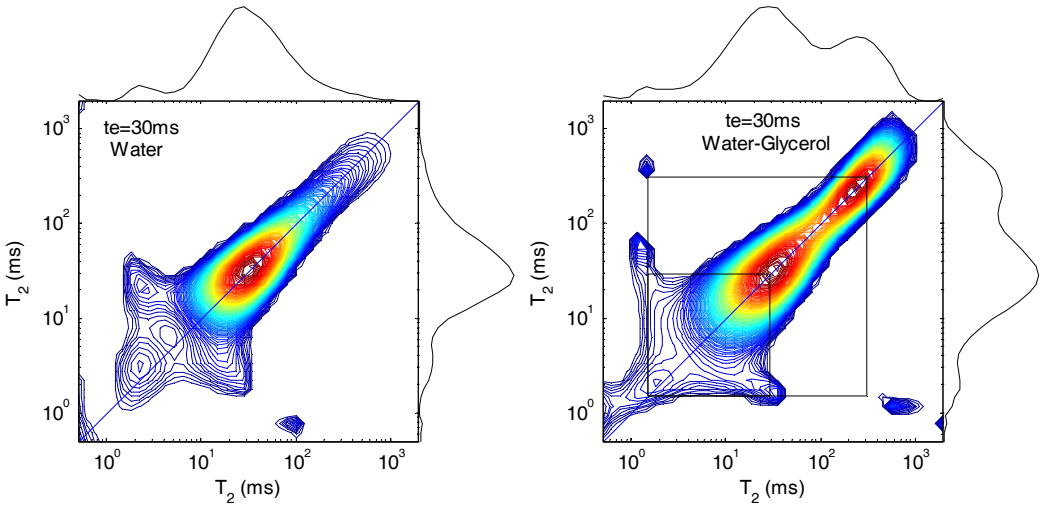

Fig. 8: T_2-store-T_2 relaxation maps for the Lavoux limestone saturated with water (left, D=2.6 10^{-9} m^2/s at 30°C) and a mixture of water and glycerol (right, D=0.18 10^{-9} m^2/s, T_{2bulk}=380 ms at 30°C). The squares highlight the exchange between micro and mesopores, and micro and macropores. When saturated with water, the T_2 distribution is wide and quasi-unimodal, in contradiction with the MICP distribution and the SEM visualization in Fig. 7. For a lower molecular diffusion of the saturating fluid, the pore coupling decreases and a multimodal distribution is observed.

CONCLUSIONS

Diffusional coupling is a very common mechanism, potentially perturbing the interpretation of 1D relaxation time distributions, but providing new information of the connectivity of porous systems. For bimodal systems in which we cover a range of pore sizes from 1 nm up to 100 μm, we defined a coupling parameter α comparing the average exchange rate and the relaxation rate of the smallest pore population (micropore) having the largest specific surface. Based on an analytical solution, we analyzed the behaviour of 1D T_2 and 2D T_2-store-T_2 relaxation experiments as a function of α. In 1D experiments and for increasing values of α, the relaxation time of micropores is shifted to smaller values and their amplitude decreases. The coupling parameter, which is proportional to the diffusivity of the saturating fluid, must vary by two orders of magnitude to switch from a weakly to a strongly coupled state.

The coupling was evidenced and quantified on a flocculated smectite gel and a shaly sandstone. Although relatively simple, the two pore population model allows the analysis of distributed bimodal systems. On complex carbonate structures, multiple exchanges were observed and explained with the help of SEM visualizations but the two pore population model could not be used for a quantitative analysis of molecular exchange. We suggest that this difficulty is either due a distribution of exchange times or the partial exchange of macro pore water with microporosity in the case of large pores. An estimate of the order of magnitude of the coupling degree is performed by changing the diffusivity of the saturating liquid by a factor of ten.

ACKNOWLEDGMENTS

The samples used in the present work were part of the Ph.D. study of M. Han focusing on electrical properties. We thank P. Levitz and J.P. Korb for fruitful discussions on the subject, and Y. Santerre for providing the thin sections.

APPENDIX 1

Coefficients included in Eq. (6) describing the dependence of the on and off-diagonal peak amplitudes as a function of storage time t_e.

$$C_1 = (A_2^- - F_2)[A_1^-(A_2^- M_a^0 - G_2 M_b^0) - G_1(B_2^- M_b^0 - F_2 M_a^0)] + (B_2^- - G_2)[B_1^-(B_2^- M_b^0 - F_2 M_a^0) - F_1(A_2^- M_a^0 - G_2 M_b^0)]$$

$$C_2 = (A_2^- - F_2)[A_1^+(A_2^- M_a^0 - G_2 M_b^0) + G_1(B_2^- M_b^0 - F_2 M_a^0)] + (B_2^- - G_2)[B_1^+(B_2^- M_b^0 - F_2 M_a^0) + F_1(A_2^- M_a^0 - G_2 M_b^0)]$$

$$C_3 = (A_2^+ - F_2)[A_1^-(A_2^+ M_a^0 - G_2 M_b^0) + G_1(B_2^+ M_b^0 + F_2 M_a^0)] + (B_2^+ + G_2)[B_1^-(B_2^+ M_b^0 + F_2 M_a^0) - F_1(A_2^+ M_a^0 + G_2 M_b^0)]$$

$$C_4 = (A_2^+ + F_2)[A_1^+(A_2^+ M_a^0 + G_2 M_b^0) + G_1(B_2^+ M_b^0 + F_2 M_a^0)] + (B_2^+ + G_2)[B_1^+(B_2^+ M_b^0 + F_2 M_a^0) + F_1(A_2^+ M_a^0 + G_2 M_b^0)]$$

$$C_5 = (A_2^+ + F_2)[A_1^-(A_2^- M_a^0 - G_2 M_b^0) - G_1(B_2^- M_b^0 - F_2 M_a^0)] + (B_2^+ + G_2)[B_1^-(B_2^- M_b^0 - F_2 M_a^0) - F_1(A_2^- M_a^0 - G_2 M_b^0)]$$

$$C_6 = (A_2^+ + F_2)[A_1^+(A_2^- M_a^0 - G_2 M_b^0) + G_1(B_2^- M_b^0 - F_2 M_a^0)] + (B_2^+ + G_2)[B_1^+(B_2^- M_b^0 - F_2 M_a^0) + F_1(A_2^- M_a^0 - G_2 M_b^0)]$$

where $A_{1,2}^{+/-} = \dfrac{s_{1,2}^{+/-} + R_{1,2}^a + k_a}{s_{1,2}^{+/-} - s_{1,2}^{-/+}}$ $B_{1,2}^{+/-} = \dfrac{s_{1,2}^{+/-} + R_{1,2}^b + k_b}{s_{1,2}^{+/-} - s_{1,2}^{-/+}}$ $F_{1,2} = \dfrac{k_a}{s_{1,2}^- - s_{1,2}^+}$ $G_{1,2} = \dfrac{k_b}{s_{1,2}^- - s_{1,2}^+}$

REFERENCES

[1] Kleinberg R.L., W. E. Kenyon, P. P. Mitra, J. Magn. Reson., Ser. A 108 (1994) 206.
[2] Ramakrishnan T.S., L.M. Schwartz, E.J. Fordham, W.E. Kenyon, D.J. Wilkinson, The Log Analyst, 40-4 (1999) 260.
[3] Anand V., G. J. Hirasaki, Petrophysics 48-4 (2007) 289.
[4] Anand V. , G. J. Hirasaki, M. Fleury, Petrophysics 49-4 (2008) 362.
[5] Mc Connell H., J. Chem. Phys. 28 (1958) 430.
[6] Orell K.G., in: D.M. Grant, R.K. Harris (Eds.), Encyclopedia of Nuclear Magnetic Resonance, John Wiley & Sons, 1996, p. 4856.
[7] Monteilhet L, J.-P. Korb, J. Mitchell, P.J. McDonald, Phys. Rev. E 74 (2006) 061404
[8] Wahsburn K.E., P.T. Callaghan, Phys. Rev. Lett. 97 (2006) 175502
[9] Song Y.Q., L. Zielinski, S. Ryu, Phys. Rev. Let. 100 (2008) 248002
[10] Guichet X., M. Fleury, E. Kohler, J. Coll. Int. Sci. 327 (2008) 84.
[11] Dunn K.J., D.J. Bergman, G.A. La Torraca, Nuclear Magnetic Resonance: Petrophysical and Logging Applications, Pergamon, 2002.
[12] Fleury M., Y. Santerre, B. Vincent, Proceeding of the SPWLA Annual Symposium, Austin, June 3-6, 2007.